Joint geophysical observations of ice stream dynamics

S. Danesi[1], M. Dubbini[2], A. Morelli[1] and L. Vittuari[3]

1) Istituto Nazionale di Geofisica e Vulcanologia, Sezione Bologna

Via Donato Creti, 12 – 40128 Bologna IT

Email: danesi@bo.ingv.it, morelli@bo.ingv.it

Tel: +39 051 4151472

Fax: +39 051 4151499

2) Università di Modena e Reggio Emilia, DiMec

Via Vignolese 905 - 41100 Modena IT

Email: marco.dubbini@unimo.it

Tel: +39 059 2056297

Fax: +39 059 2056126

3) Università di Bologna, DISTART

Viale del Risorgimento, 2 – 40136 Bologna IT

Email: luca.vittuari@mail.ing.unibo.it

Tel: +39 051 2093103

Fax: +39 051 6448073

Abstract

Ice streams play a major role in the ice mass balance and in the reckoning of the global sea level; they have therefore been object of wide scientific interest in the last three decades. During the 21st Italian Antarctic Expedition, in the austral summer 2005-06, we deployed a joint seismographic and geodetic network in the area of the David Glacier, Southern Victoria Land. This campaign followed a similar experiment carried out in the same area during the austral summer 2003-04 with the deployment of a seismographic network that recorded significant microseismicity beneath the David Glacier, primarily occurring as a few small clusters. In the latest 2005-06 deployment, 7 seismographic stations and 3 GPS geodetic receivers operated continuously for a period of 3 months (November 2005-early February 2006) in an area of about 100x150 km^2 around the David Glacier. We have carried out several analyses using the combined data sets. These included the examination of the temporal evolution in earthquake magnitude and location and also the contemporaneous observation of both seismic activity and surface kinematics of the ice stream to possibly correlate the recorded microseismicity with the movement of the glacier, affected by the Ross Sea tides. Here we present some details of the two temporary networks and preliminary results and implications.

Introduction

Ice streams are the fast flowing channels through which polar sheets pour ice into surrounding oceans and influence their mass balance, thermal regime and circulation with evident consequences on large-scale climate changes, since global sea level is basically regulated by mass variations in Greenland and Antarctic ice sheets. From mass balance studies it has been inferred and generally accepted that the complete melt of polar ice would potentially result in a dramatic sea level rise (about 70m) [Rignot and Thomas, 2002; Alley et al., 2005].

One fundamental grasp of the past 30 years is that the response of polar ice sheets to climate changes is far from being slow and steady; on the contrary ice sheets are extremely sensitive to global warming, with rapid dynamic feedback on ice flow and consequent pronounced variations in mass balance. For this reason, the understanding of ice stream mechanics and the measurement of flow variations are valid gateways towards the study of ice sheet (and climatic) stability.

The David Glacier and the Drygalski Ice Tongue (its 100km-long floating seaward extension) represent the main structure of the very complex drainage system of the Victoria Land area. The glacier has two main tributaries, flowing from DomeC and Talos Dome, which converge downstream of the grounding line, after a remarkable icefall due to a subglacial ridge crossing the ice flow and after a large basin called David Cauldron (Figure 1).

Several glaciological studies have been done over the last decades to detect the grounding line location and to study the floating ice tongue profile. The grounding line was initially thought at the mouth of the glacier bay, then it was revised further upstream at the David Cauldron and finally it was positioned 15 km upstream following the results of InSAR observations [Frezzotti, 1993; Frezzotti et al., 2000; Rignot, 2002].

At the grounding line, the glacier base is about 3 km below the sea level and loses 68% of its mass from bottom melting within 20 km of the grounding line, driving an up-welling of “super-

cooled" water that allows the deposition of enough marine ice to preserve the length of the Drygalski Ice Tongue [Frezzotti et al., 2000, Rignot and Jacobs, 2002].

During the 2005-06 Austral Summer, we carried out an observational campaign in the area of the David Glacier (South Victoria Land, Antarctica) with the aim of collecting simultaneous time series of geodetic and seismological data.

The target of the experiment is the study of possible correlations between vertical/horizontal displacements of the glacier and the weak typical seismic activity inland beneath the glacier. Location of seismographic and geodetic stations operating in the David area are listed in Table 1 and shown in Figure 1 (stars and circles respectively).

The Global Navigation Satellite System (GNSS) takes advantage of satellite positioning techniques to provide accurate positioning information with reliable time reference.

It has been shown that the use of GNSS instrumentations can be very useful for the measurement of glaciers movements [Hulbe and Whillans, 1994; Frezzotti et al., 1998] and it is one of the most reliable methods to monitor the position of selected points located on a glacier with high precision. Moving glaciers can also be monitored in a seismological perspective. Seismic signals related to glacier motion have been observed since early '70s [Neave and Savage, 1970; Van Wormer and Berg, 1973] obtaining increasing interest over the last decades among the scientific communities. Actually, seismic activity originated beneath fast flowing ice streams has been recorded both in Greenland and in Antarctica with fairly different characteristics. From the study of surface seismic waves, Ekström et al. [2003, 2006a, 2006b] have identified a number of glacier-related earthquakes, with magnitude higher than 4.5 that can be modelled with glacial-sliding slips mainly located beneath flowing glaciers. They have observed a remarkable increase in the number of such events between 2002 and 2005 as a consequence of significant changes in the glacial flow owing to late global warming. Differently then in Greenland, in Antarctica low-magnitude seismicity is most commonly recorded and located beneath ice streams either associated with repeating stress release across small sticky patches or basal drag regime [Bahr and Rundle, 1996, Alley, 2000; Smith, 2006].

Seismological Campaign

Data Collection and Analysis

The best-studied system of Antarctic ice streams is located in the Siple Coast, the western coast of the Ross Ice Sea. Over the past 20 years [Blankenship et al., 1986; Alley et al., 1986], a number of geophysical observations have been held in the area providing deeper understanding about the dynamics of fast flowing ice streams and climatic implications in a global sense [Alley et al., 2005; Horgan and Anandakrishnan, 2006].

In the David Glacier area, on the eastern side of the Ross Embayment, a low-energy but significant seismic activity was revealed during the 1999-2000 seismological campaign that was carried out by a joint Australian and New Zealand project in the central Transantarctic Mountains area [Bannister and Kennett, 2002]. The glacier was more than 200 km far from the network target area, therefore the events were initially located with some uncertainties (owing to the unbalanced azimuthal coverage of the array) and possibly ascribed either to the presence of a large regional right-lateral lineament beneath the David Glacier [Salvini and Storti, 1999] or to stick-slip motion at the base of the ice stream basically driven by basal shear stress [Bannister and Kennett, 2002].

Afterward, the David Glacier was the target area for 2 seismological campaigns: the first was jointly held by Italy and New Zealand during the 2003-04 Austral Summer (19th Italian Expedition) [Danesi et al., 2007 (DBM07)], the second was carried out by the Italian group during the 2005-06 Austral Summer (21st Italian Expedition) with simultaneous seismic and GPS observations.

Figure 1 shows the sites where autonomous remote seismographic stations were installed in 2005-06 (green stars). The stations were sited on rock outcrops surrounding the glacier (some were re-occupied after the first expedition) and operated continuously over 3 months recharged by photovoltaic panels. Each site was equipped with a 3-component broadband seismometer Trilium40 and a Reftek 130-01 digital recorder/data logger with 125sps fixed (Figure 2a). The

array covered an area of about 100x150 km^2 around the David Glacier, from the coastline toward the first peaks of the Transantarctic Mountains (Figure 1).

After data retrieval and detection of seismic episodes with trigger algorithms, we identified more than 10000 low energy events distributed on three main classes.

The array successfully recorded teleseismic signals, mainly originated along the peri-Antarctic spreading oceanic ridges.

Then, we principally recorded episodes originating within the ice layer that we call *icequakes* hereinafter. Their seismic signal is strongly impulsive, short in duration, rich in high frequencies and rapidly attenuating (Figure 3), reason why they are usually recorded by only one or two close stations and can be hardly or not at all located. Hundreds of icequakes per day testify that these are the most common and frequent occurrence in glacial environments: fractures can originate and propagate through the ice owing to crevasses, steep changes in bedrock topography, walls and asperities dragging effects, inhomogeneous strain in the flow, iceberg calving or combinations of several causes. Typically, icequakes are local effects of the glacier flow.

However, the most interesting events are of a third class. They occurred at the bedrock-ice interface with more than 150 occurrences that will be referred to as *basal events* hereinafter. The characteristic signal of basal events shows weak P and S arrival, duration of a few tens of seconds and spectra rich in low frequencies (Figure 4).

After a preliminary determination of hypocentres using the HYPOINVERSE algorithm [Klein, 2002], we determined the accurate location of basal events with the Double-Difference (DD) method of Waldhauser [2001] which provides high precision relative locations (see method description in DBM07). The spatial distribution of epicentres is plotted in Figure 5: red and green stars represent events recorded respectively during the first (Nov 2003 - Jan 2004) and the second experiment (Nov 2005 – Jan 2006). Note that all the episodes occurred along the main branch of the David Glacier, that is the southern, faster, stream draining DomeC and no events were detected in the slower tributary flowing from Talos Dome.

Seismic occurrences are clustered in space and generally concentrated around the main icefall (Figure 5), allowing us to exclude a tectonic origin eventually related to the presence of an active fault and pointing to a glacial-related source. Following DBM07, we distinguish 3 main groups of basal events depending on their location referred to the icefall: Upstream North (UP-N), Upstream-South (UP-S) and Downstream (DW).

Upstream events

The UP-N and UP-S clusters count together 74 events occurring sparsely at the top of the icefall, in correspondence of the area where the ice flows fast (more than 500 m/y from Frezzotti et al., 1998), the bedrock topography drops 300-400 m and the mean slope is around 60%-80% [Rignot, 2002].

Following the procedure explained in DBM07, we found the Mw magnitude for all the events as shown in Figure 6 where orange and green bars represent the magnitude distribution vs. event count for UP clouds (2003-04 and 2005-06 respectively).

The events observed in this study have magnitude ranging between 1.1 and 2.3, generally do not indicate evident foreshock/aftershock pattern and do not follow the typical Gutenberg-Richter distribution of magnitude–frequency scaling [Gutenberg and Richter, 1944].

Changes in topography have a major influence on glacier dynamics, as the basal shear stress at the glacier bed σ_b depends on both ice thickness *h* and surface slope α as $\sigma_b = \rho g h \sin\alpha$, where ρ is the density of ice and *g* is gravity.

The coupling between a moving glacier and its bedrock is generally a highly non linear problem with basal shear stress depending upon ice plastic properties, till deformation, characteristics of sediments beneath the till, basal melt rate, basal topography and roughness at the ice-till interface.

Nevertheless, if we assume a remarkable effect of abrasion over the bedrock at the top of the icefall, owing to the steep slope and the fast sliding flow, we can neglect the sediments and their

deformation and expect the movement of a lubricated glacier on the bedrock will be primarily controlled by ice deformation.

Provided realistic values for parameters involved in the equation, the basal shear stress at the ice-rock interface is:

$$\sigma_b = \rho g h \sin\alpha \approx 2.25 MPa$$

where:

ρ= 917 kg·m^{-3}, g= 9.81 m·s^{-2}, h= 500 m, sin$\alpha \approx$ 0.5.

An increase in basal shear stress may result in further formation of melt-water at the interface and may favour sliding speed, eventually causing a partial decoupling of the glacier from the bed. On the other hand, obstacles distributed on the bedrock will experience higher drag forces and may originate stick-slip seismic episodes.

Downstream events

75 epicentres in the DW cluster occurred in an extremely tight cluster of less than 2 km^2, where glacier likely deviates its flow forced by the presence of topographic boundary (Figure 5). Cross-correlations between waveforms for event pairs above 0.95 [DBM07] indicate extremely small separations between the hypocentres and impressing similarity in waveforms (Figure 7). Moment magnitudes Mw are plotted in Figure 6 with red bars revealing a Gaussian-like frequency distribution centred at Mw≈1.4.

The extremely high similarity of hypocentres, waveforms and magnitudes for DW events, implies that the source process cannot be purely ascribed to the sliding friction on the bedrock, but rather suggests the presence of an asperity on the ice–bedrock interface, that repeatedly breaks with a characteristic length.

An isolated asperity, resistant to the ice flow and acting as a sticky-spot, would account for local higher concentration of shear stress and occurrences of recurring, almost identical, episodes. Our estimate of the cumulated slip provided by the DW events over a full year would be in the order of 16m [DBM07] representing no more than 2.5% of the annual glacier motion inferred from

GPS measurements. Therefore, the basic process by which the flow moves past the asperity is not the seismic slip but its plastic ice deformation around the obstacle. Episodically, the DW patch experiences brittle failure and, when it slips seismically, the seismic episode is always associated with the same energy and characteristic length.

Interestingly, none of the events recorded during the 2005-06 campaign (green stars in Figure 5) was located in the area of the DW cluster, suggesting that the sticky-spot would be no longer active either due to the possible abrasion and smoothing of the patch or to higher basal lubrication.

In the latter case, we might expect an increasing flow speed with respect to previous horizontal velocity observations. GPS data collected in the David Cauldron (site ICF1 in Figure 1) during the 2005-06 austral summer reveal that the flow speed in this point was 1.6 m/day (see next section) but, unfortunately, we don't have any direct GPS measurement available for the 2003-04 ice flow velocity. Frezzotti et al. [1998] measured the mean ice speed between 1991 and 1994 some km downstream of ICF1 founding a slightly lower value of 1.39 m/day (their station Da4).

The two measures cannot be directly compared because the glacier traces a sharp S-shaped turn between ICF1 and Da4 but we can reasonably think that the flow will reduce its speed before bending and will slowly accelerate again after the corner. Bearing in mind that it is not possible to correlate the two measures exactly, the essential point at this level is their compatibility.

GPS Campaign

In order to follow the kinematics of the David-Drygalski, two temporary GPS geodetic stations were installed on the glacier at points ICF1 and DRY1 (Figure 1), in November 2005 and in January 2006 respectively.

We used dual frequency Trimble5700 GPS receivers equipped with Zephyr and Zephyr Geodetic antennas and 1Gb removable memory cards; each antenna was tightened to the head of an aluminium pole (well driven into the ice) and acquisition parameters were set with measurement rate 15 s, elevation mask 13° and daily sessions (Figure 2b).

The equipment was prepared to operate continuously, using solar energy for battery charging. The first point (ICF1) was installed at the bottom of the icefall, as close as possible to the epicentral area of the DW cluster of earthquakes previously described, compatibly with severe crevassing; the second point (DRY1) was installed on the floating ice tongues at the bottom of Hughes Bluff outcrop (red circles in Figure 1).

As primary master station for the kinematic processing, a GPS receiver was installed on a 3-D benchmark fixed into the rocky outcrop Hughes Bluff, but in order to insert the measurements within the International Terrestrial Reference Frame (ITRF2000), we also used simultaneous GPS acquisitions from the GPS permanent station located at the Mario Zucchelli Station (TNB1).

Kinematic GPS is a satellite-based relative survey method that allows for the evaluation of a moving receiver trajectory with respect to a reference station. Using this method, accuracies in a range of few centimetres in relative positioning are achievable. In a classical carrier phase differenced approach, positioning reliability is mainly related to the correct setting of unknown phase ambiguities as integer numbers. Therefore the problem of the area coverage is related to ambiguity resolution, which is typically possible in the range of limited distances (generally speaking 15-30 km) from a reference station. On wider ranges the solution becomes more disturbed owing to the de-correlation of systematic effects in the GPS measurements and particularly at high latitudes, where the presence of large ionospheric activities causes significant scintillation effects on the GPS signal.

The Drygalski Ice Tongue fluctuates forced by the Ross Sea tide. One of our goals was the investigation on the effect of the ocean tide on the ice tongue vertical and horizontal movements. Unfortunately, we couldn't observe any direct correlation between tidal forcing and seismic occurrences because we didn't registered any earthquake in the DW area during the GPS campaign.

An analysis of discontinuous measurements acquired in 1991, 1994 and 1995 by tide gauges installed at MZS, reveals that the stability values of the major components of ocean tides (O_1, K_1, Q_1, M_2, S_2 and N_2) ranges from 99.6% to 100%. The other components (M_4, M_3, MN_4,

μ_2, M_4, MO_3, L_2, M_6 and $2MS_6$) show stability values in the range 80-97%. These 15 harmonic constants can nearly completely account for amplitude values [Capra et al., 1999]. The tide character expressed by the ratio of the sums of amplitudes (O_1 and K_1 with respect to M_2 and S_2) is 2.72, therefore the dominant pattern of the tide is diurnal, with small semi-diurnal components. This means that during a lunar day (24 hours and 50 minutes) there is only one high tide and only one low tide with a clear spring-to-neap tidal cycle.

Unfortunately a technical problem occurred at the reference station Hughes Bluff in the period 024/06-030/06 and so we processed the ionosphere-free (LC) observable double-differenced with respect to the Italian permanent station TNB1 which is continuously operative at the Italian scientific station MZS. Due to the long distance between the David-Drygalski and TNB1 (more than 100 km), the noise level observed in relative positioning is about one decimetre.

Data processing of Antarctic long-range kinematic acquisition requires the development of strategies especially tuned for each experiment. In order to manage the effects of such stringent constraints, we adopted the open scientific GPS data processing software Gamit/Globk package [King and Bock, 2005] and in particular in this work we analyzed twelve days of contemporaneous GPS observations at DRY1 and ICF1 using the kinematic module TRACK version 1.15 [Chen, 1998; Herring, 2002; Herring et al., 2006].

In the data analysis process we computed site positions by means of RINEX format (Receiver INdependent Exchange) data files and precise ephemeris post-calculated by the IGS (International GNSS Service) using global data.

In the last version (1.15) of TRACK, a tool for antenna phase-centre mapping has been implemented so that the software is also able to read the file of absolute calibration (e.g. igs05_1402.atx). TRACK allows for the use of different strategies of analysis depending on the site distance from the reference master station. In our case, the length of the baselines is about 100 Km and the differential ionospheric and tropospheric delays are very high. For this reason, the software uses a floating-point estimate technique and ionospheric delay constraint to LC

observable (the Melbourne-Webbena linear combination is often used to resolve L1-L2 ambiguities and several different approaches to determine L1 and L2 cycles separately).

In Figure 8 we report the comparison between vertical components derived by GPS kinematic solutions (computed every 15 s) at points ICF1 and DRY1 and the predicted ocean tide values, computed in the same period adopting the 26 harmonic constants estimated at MZS.

The vertical motion at point DRY1 with periodic undulations up to 70cm (Figure 8) demonstrates the clear response of floating ice-tongue to the sea tide. On the other hand, the amplitude of vertical motion at point ICF1 is strongly reduced, suggesting that ICF1 is constrained and located close to the grounding line, possibly 1-2km upstream of the grounding line if compared with InSAR interpretations [Rignot, 2002].

The horizontal velocities of the Drygalski Ice-tongue vary as well as a function of time with respect to tidal amplitudes: in the two-week acquisition time, the extent of speed amplitude with respect to spring-to-neap cycles decreased till a neap tide and increased during the period that preceded the spring tide (Figure 9).

GPS data collected during the observed period of the 2005-06 austral summer reveal that the average horizontal flow speed was 1.6 m/day (ca 580m/y) at point ICF1 with azimuth 42° 57', and 1.48 m/day (ca 540 m/y) with azimuth 101° 15' at point DRY1.

Discussion and Conclusions

The deployment of seismographic and geodetic temporary stations around the David Glacier allowed us to collect simultaneous time series of data and to analyze them jointly.

Low-magnitude seismic occurrences at the ice-bedrock interface are common, but high concentration of shear stress is purely due to basal friction or to the presence of bedrock asperities acting as sticky-spots. In fact, epicentres are either spread at the top of the icefall (where the mean slope is around 60%-80%) or focused in small clusters, which would reveal the presence of basal patches. Nevertheless, isolated asperities would not affect significantly the

stability of the ice stream, but rather sliding, creeping and basal deformations would account for most of the glacier motion.

GPS observations at the two sites placed after the icefall reveal that both vertical and horizontal glacier displacements are largely forced by the Ross Sea tides. Unfortunately, none of the events occurring during the GPS campaign were located in the same area, so we couldn't verify possible correlations between the tide and the seismic triggering.

As expected, the vertical motion of the floating tongue (site DRY1) is wholly correlated, in phase and amplitude, with the predicted tide (Figure 8). On the contrary, the major movement at ICF1 is descendent with only moderate oscillations, so we can infer that the glacier is still anchored at the bedrock in that point, upstream of the grounding line.

Interestingly, the dominant diurnal ocean tide also regulates horizontal velocities of the ice stream with a clear temporal variation correlated with the spring-to-neap tidal cycle (Figure 9). Longitudinal perturbations propagate rapidly over large distances, a conclusion that is supported by several previous studies [Payne and others, 2004; Gudmundsson, 2006]. In fact, the tidal oscillation acts as a vertical stress modulator: neap and spring tide correspond respectively to reduction and increment of vertical stresses (and glacier weight) on the bedrock, making the ice flow faster or slower. It is worth noting that amplitude variations at ICF1 are not in phase with the tide: the delay might be introduced as combined effect of plastic necking upstream of the grounding line and possible variable transfer of water filling cavities where the glacier decouples from its bed and begins to float.

Our estimate of ICF1 horizontal velocity is in good agreement with InSAR evidences: the site would be located inland, between the InSAR equal-velocity 500 and 600 m/y contour lines reported in Rignot [2002] which is confirmed by our estimate of 580m/y for horizontal motion.

GPS data collected during the 2005-06 austral summer reveal that the flow speed generally agrees with data collected between 1991 and 1994 by Frezzotti et al. (1998): in particular, the horizontal velocity measured in 1991-1994 at point Da2 (1.51 m/day) located at S 75° 21' 45", E

162° 08’ 58” is quite confirmed by the new GPS measurements carried out at point DRY1 eleven years later (Figure 9).

In line with recent observations [Shepherd and Wingham, 2007], these results may suggest that the average flow of the glacier has not varied significantly over the last decade in terms of flow horizontal velocities: in a time when polar areas are generally experiencing increasing instability owing to late global warming, the East Antarctic Ice Sheet still exhibits positive mass balance, contributing to moderate the sea-level rise.

References

1. Alley R.B., D.D. Blankenship, C.R. Bentley & S. T. Rooney, 1986, *Deformation of till beneath ice stream B, West Antarctica,* Nature, 322, 6074, 57-59. doi:10.1038/322057a0
2. Alley, R.B., 1992, *Sticky spots under ice streams,* Antarctic Journal of the U.S., 28(5), 50-51.
3. Alley R.B., P.U. Clark, P. Huybrechts & I. Joughin, 2005, *Ice-sheet and sea level changes*, Science, 310, 456-460.
4. Bahr D.B. & J.B. Rundle, 1996, *Stick-slip statistical mechanics at the bed of a glacier*, Geophys. Res. Lett., 23, 16, 2073-2076.
5. Bannister S. & B.L.N. Kennett, 2002, *Seismic Activity in the Transantarctic Mountains – Results from a Broadband Array Deployment*, Terra Antarctica, 9, 1, 41-46.
6. Blankenship D.D., C.R. Bentley, S.T. Rooney & R.B. Alley, 1986, *Seismic measurements reveal a saturated porous layer beneath an active Antarctic ice stream*, Nature, 322, 6074, 54-57. doi:10.1038/322054a0.
7. Capra A., S. Gandolfi, C. Lusetti, C. Stocchino & L. Vittuari, 1999, *Kinematic GPS for the study of tidal undulation of floating ice tongue*, Bollettino di Geodesia e Scienze Affini, IGM, LVIII, n. 2, 151-173.
8. Chen, G., 1998, *GPS Kinematic Positioning for the Airborne Laser Altimetry at Long Valley, California,* Ph. D. Thesis, Massachusetts Institute of Technology, pp.173, Cambridge, MA.
9. Danesi S., S. Bannister & A. Morelli, 2007, *Repeating earthquakes from rupture of an asperity under an Antarctic outlet glacier*, Earth and Planet. Sc. Lett., 253, 1-2, 151-158.
10. Ekström G., M. Nettles and G.A. Abers, 2003, *Glacial earthquakes*, Science, 302, 622-624.
11. Ekström G., M. Nettles & V.C. Tsai, 2006a, *Seasonality in Increasing Frequency of Greenland Glacial Earthquakes*, Science, 311, 1756-1758.

12. Ekström G., 2006b, *Global detection and Location of Seismic Sources by Using Surface Waves*, Bull. Seismol. Soc. Am., 96, 4A, 1201-1212.
13. Frezzotti, M. 1993. *Glaciological study in Terra Nova Bay, Antarctica, inferred from remote sensing analysis*, Ann. Glaciol. 17, 63-71.
14. Frezzotti M., A. Capra & L. Vittuari, 1998, *Comparison between glacier ice velocity inferred from GPS and sequential satellite images*, Ann. Glaciol., 27, 54-60.
15. Frezzotti, M., I.E. Tabacco & A. Zirizzotti. 2000. *Ice discharge of eastern Dome C drainage area, Antarctica, determined from airborne radar survey and satellite image analysis*, Ann. Glaciol. 46(153), 253-264.
16. Gudmundsson G.H., 2006, *Fortnightly variations in the flow velocity of Rutford Ice Stream*, West Antarctica, Nature, 444, 7122, 1063-1064.
17. Gutenberg B. & C.F. Richter, *Frequency of earthquakes in California*, 1944, Bull. Seismol. Soc. Am., 34, 185–188.
18. Herring T.A., 2002, *Track GPS kinematic positioning program*, Version 1.07. Cambridge, MA: Massachusetts Institute of Technology.
19. Herring T.A., R. King & S. McClusky, 2006, *Gamit Reference Manual, release 10.3,* Report Massachusetts Institute of Technology, Cambridge, MA.
20. Horgan H.J. & S. Anandakrishnan, 2006, *Static grounding lines and dynamic ice streams: Evidence from the Siple Coast, Antarctica*, Geophys. Res. Lett., 33, L18502, doi:10.1029/2006GL027091.
21. Hulbe C.L. & I.M. Whillans. 1994. *Evaluation of strain rates on Ice Stream B, Antarctica, obtained using GPS phase measurements*, Ann. Glaciol., 20, 254-262.
22. King R.W. & Y. Bock (2005), Documentation for the GAMIT GPS processing software release 10.2, Mass. Inst. of Technol., Cambridge.
23. Klein F.W., 2002, *User's guide to HYPOINVERSE-2000, a fortran program to solve for earthquake locations and magnitudes*, U.S. Geol. Survey Open File Report, 2–171.

24. Neave K.G. & J.C. Savage, 1970, *Icequakes on the Athabasca Glacier*, J. Geophys. Res., 75, 8, 1351-1362.
25. Payne A.J., A. Vieli, A.P. Shepherd, D.J. Wingham & E. Rignot, 2004, *Recent dramatic thinning of largest West Antarctic ice stream triggered by oceans,* Geophys. Res. Letts., 31, L23401.
26. Rignot E. & R.H. Thomas, 2002, *Mass Balance of Polar Ice Sheets*, Science, 297, 1502-1506.
27. Rignot E., 2002, *Mass balance of East Antarctic glaciers and ice shelves from satellite data*, Ann. Glaciol., 34, 217–227.
28. Rignot, E. & S. Jacobs, 2002, *Rapid bottom melting widespread near Antarctic Ice Sheet grounding lines,* Science, 296, 2020-2023,
29. Salvini F. & F. Storti, 1999, *Cenozoic right-lateral strike-slip tectonics in the Ross Sea region, Antarctica* in: Ricci C.A. (ed.) The Antarctic region: Geological Evolution and Processes, Terra Antarctica Publ., Siena, 585-590.
30. Shepherd A. & D. Wingham, 2007, *Recent Sea-Level Contribution of the Antarctic and Greenland Ice Sheets,* Science, 315, 1529-1532, doi:10.1126/science.1136776.
31. Smith A.M., 2006, *Microearthquakes and subglacial conditions*, Geophys. Res. Lett., 33, L24501, doi:10.1029/2006GL028207.
32. Van Wormer D. & E. Berg, 1973, *Seismic evidence for glacier motion,* J. Glaciol. 12, 65, 259-265.
33. Waldhauser F., 2001, *hypoDD — a program to compute Double-Difference hypocentre locations*, U.S. Geol. Survey Open File Report, 1–113.

Acknowledgements

We thank all the people involved in preparation, deployment and retrieval of stations and data. We also thank Stephen Bannister, a co-author in DBM07, for his help in this work. This research was conducted with field logistic and financial support provided by the Italian national

organization for research in Antarctica (PNRA S.C.r.l.).

Tables

Table 1

Position and operativeness of GPS receivers and seismographic stations used in this study.

		Latitude	Longitude	Height (m)	Station code	Operativeness (Julian day)
GPS sites	GPS HUGHES (master station)	75°23' 52.68" S	162°12'06.18" E	165.667	VL19	316/05 – 038/06
	GPS Drygalski	75°21'45" S	162°08'15" E	37	DRY1	015/06-038/06
	GPS Cauldron	75°23'07" S	160°54'06" E	201	ICF1	313/05-038/06
SEISMOGRAPHIC sites	Cape Philippi	75°13'08.80 S	162°32'40.93 E	425	PHIL	318/05 – 365/05
	Hughes Bluff	75°23'53.10 S	162°12'08.155 E	215	HUGH	316/03 – 022/04 307/05 – 033/06
	Mc Daniel	75°47'57.83 S	161°47'53.74 E	780	MDAN	332/03 – 045/04
	Morris Basin	75°39'22.51 S	159°04'19.08 E	880	MORR	341/03 – 050/04
	Mt Joyce	75°37'05.55 S	160°53'27.80 E	1230	JYCE	320/03 – 022/04 305/05 – 033/06
	Mt Priestley	75°13'25.38 S	161°54'32.37 E	475	PRST	316/03 - 021/04 312/05 – 033/06
	Ohg	75°07'57.18 S	161°07'50.05 E	630	OHG	337/03 – 050/04 321/05 – 033/06
	Starr Nunatak	75°53'56.36 S	162°35'33.235 E	70	STAR	332/03 - present
	Trio Nunatak	75°29'52.23 S	159°41'19.71 E	1145	TRIO	309/05 – 033/06

Figure Captions

Figure 1 - Reference map

A satellite image of the David Glacier (ASTER_VNIR 2003 Feb 6th) has been georeferenced to a South Pole Polar Stereographic projection. The study area is in evidence in the inset. The picture shows the deployment of the 2005-06 seismic network (green stars) and GPS receivers (red circles). TNB1 (yellow star) is the permanent geodetic Italian station operating close to the Italian scientific base MZS.

Figure 2 – Typical station installation

a) All the seismographic stations were sited on rocky outcrops around the glacier and equipped with photovoltaic panels for autonomous recharging. In the foreground the seismic sensor Trillium40 sheltered with a cover and anchored to the rock. Digitizer/data-logger RefTek 130-01, batteries and electronic regulator were protected inside the insulated grey box behind the panel.
b) Temporary GPS site on the Drygalski. A dual frequency GPS Trimble5700 receiver was equipped with 1Gb removable memory cards for data logging and batteries recharged by photovoltaic panels; a Zephyr antenna was tightened on the head of an aluminium pole well driven into the ice.

Figure 3 – Icequake seismic signal

a) Vertical component of seismic signal (in velocity) vs. time. Icequake are frequent events, have short duration and impulsive onset. b) Amplitude of frequency spectrum of icequake signal vs. frequency in hertz: maximum amplitudes are reached for frequencies higher than 10Hz.

Figure 4 – Basal earthquake seismic signal

a) Vertical component of seismic signal (in velocity) vs. time for typical basal event. The weak onset of body waves is followed by high amplitude surface waves that are amplified as reverberations within the ice layer.

b) Amplitude of frequency spectrum is rich in low frequencies, typically lower than 1Hz.

Figure 5 – Epicentral distribution

Spatial distribution of basal event epicentres related to local topography. Satellite image of the David Glacier (ASTER_VNIR 2003 Feb 6th) georeferenced to a South Pole Polar Stereographic projection. Red and green stars represent the location of events recorded respectively during the first (Nov 2003 - Jan 2004) and the second experiment (Nov 2005 – Jan 2006).

Clusters of events are labelled following DBM07: UP-N and UP-S mark respectively Upstream North and South clusters, DW is the Downstream cluster referring to the main icefall. Note that all the events occurred during the 2005-06 campaign were located at the top of the icefall, and none of them occurred in the DW area.

Figure 6 – Magnitude distribution

Distribution of occurrences with respect to moment magnitude Mw of all the basal events. Colours are different for events of different clusters: red bars refer to DW events, orange bars refer to UP events (first Campaign), and green bars refer to UP events of the second Campaign.

Figure 7 – DW seismic signals

Vertical components of seismograms for 11 different events, as recorded by a seismometer station 34 km WSW of the cluster. The similarity between waveforms for the different events is impressive.

Figure 8 – GPS Vertical Displacements

ICF1 and DRY1 ellipsoidal heights derived by kinematic GPS solutions as a function of time, with respect to predicted sea tide.

Figure 9 – GPS Horizontal Displacements

ICF1 and DRY1 horizontal velocity measured by kinematic GPS approach. The picture compares predicted ocean tide and horizontal speed of GPS points, showing that speed variation with time depends on tidal amplitude.

161°00' E
162°00' E
163°00' E
164°00' E
165°00' E
166°00' E
74°30' S
75°00' S
75°30' S
76°00' S
160°00' E
159°00' E
0 5 10 20 30 40
Kilometers
TNB1
flow from Talos Dome
OHG
PRST
PHIL
DRY1
HUGH
David Cauldron
Ice Fall
ICF1
flow from DomeC
TRIO
JYCE
STAR
Study region

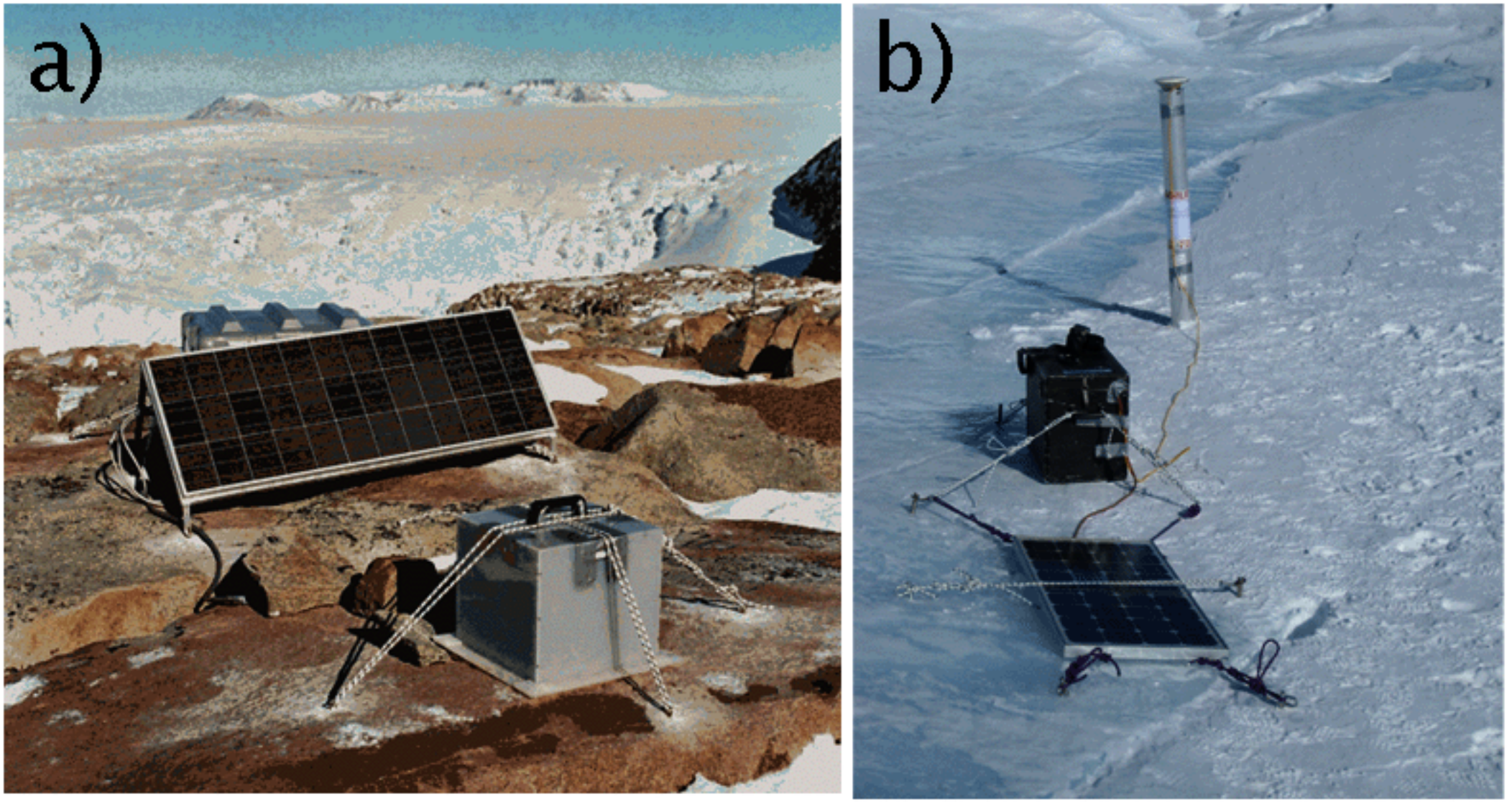
a)
b)

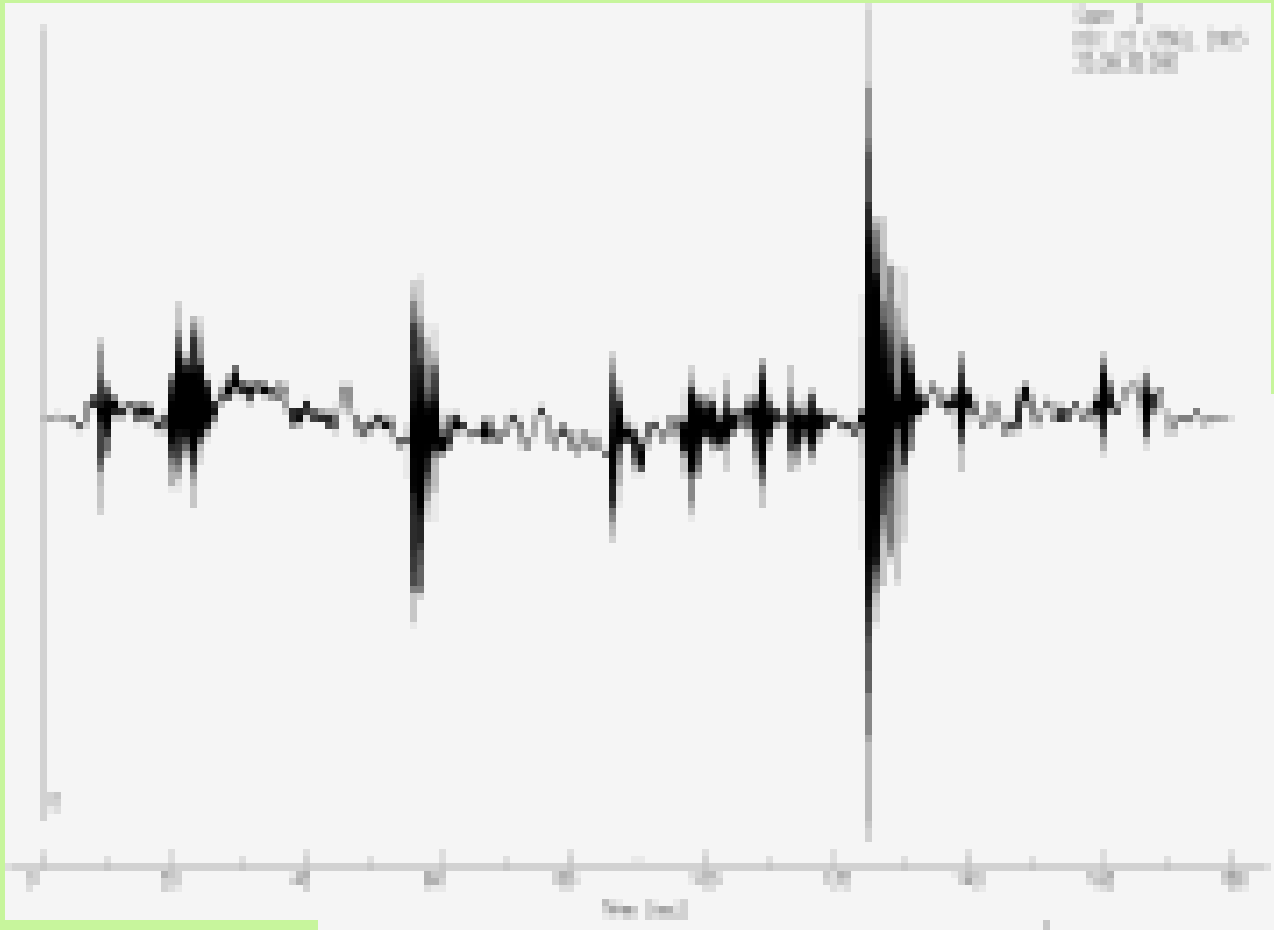

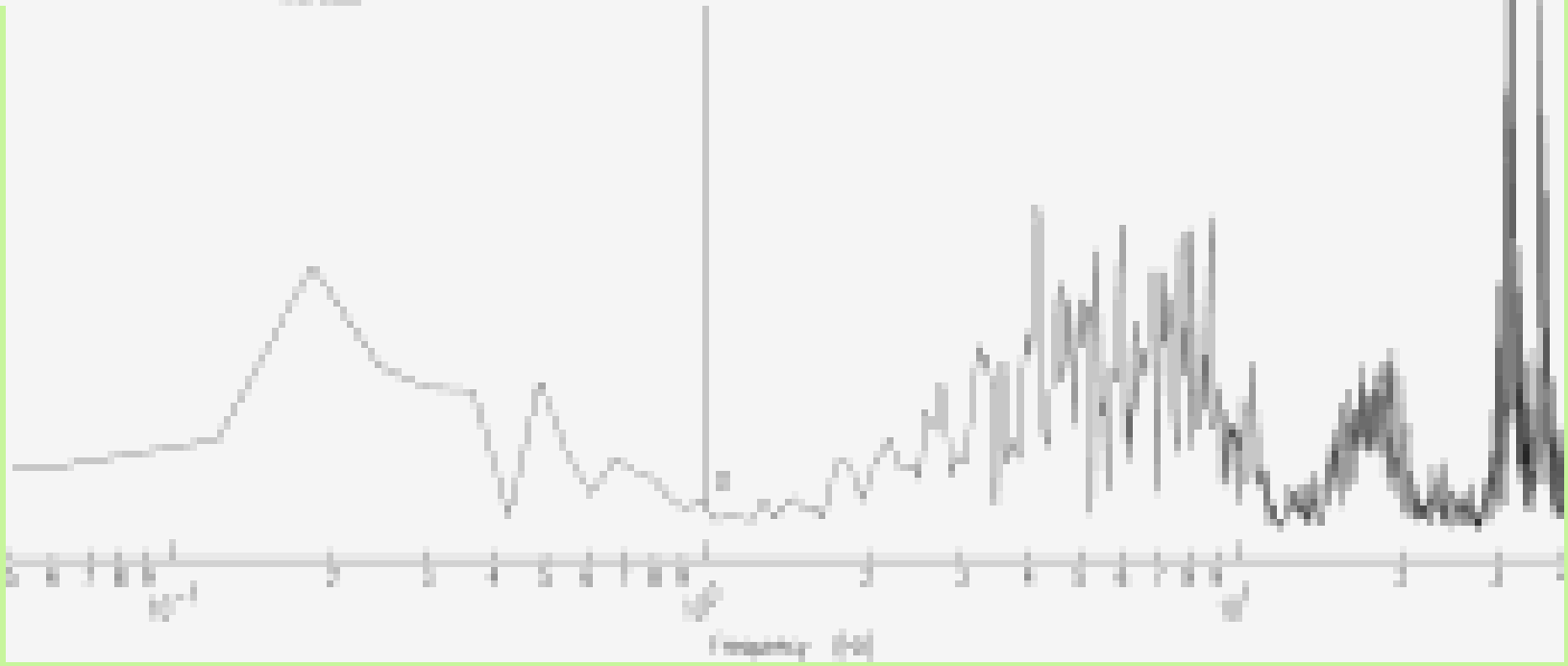

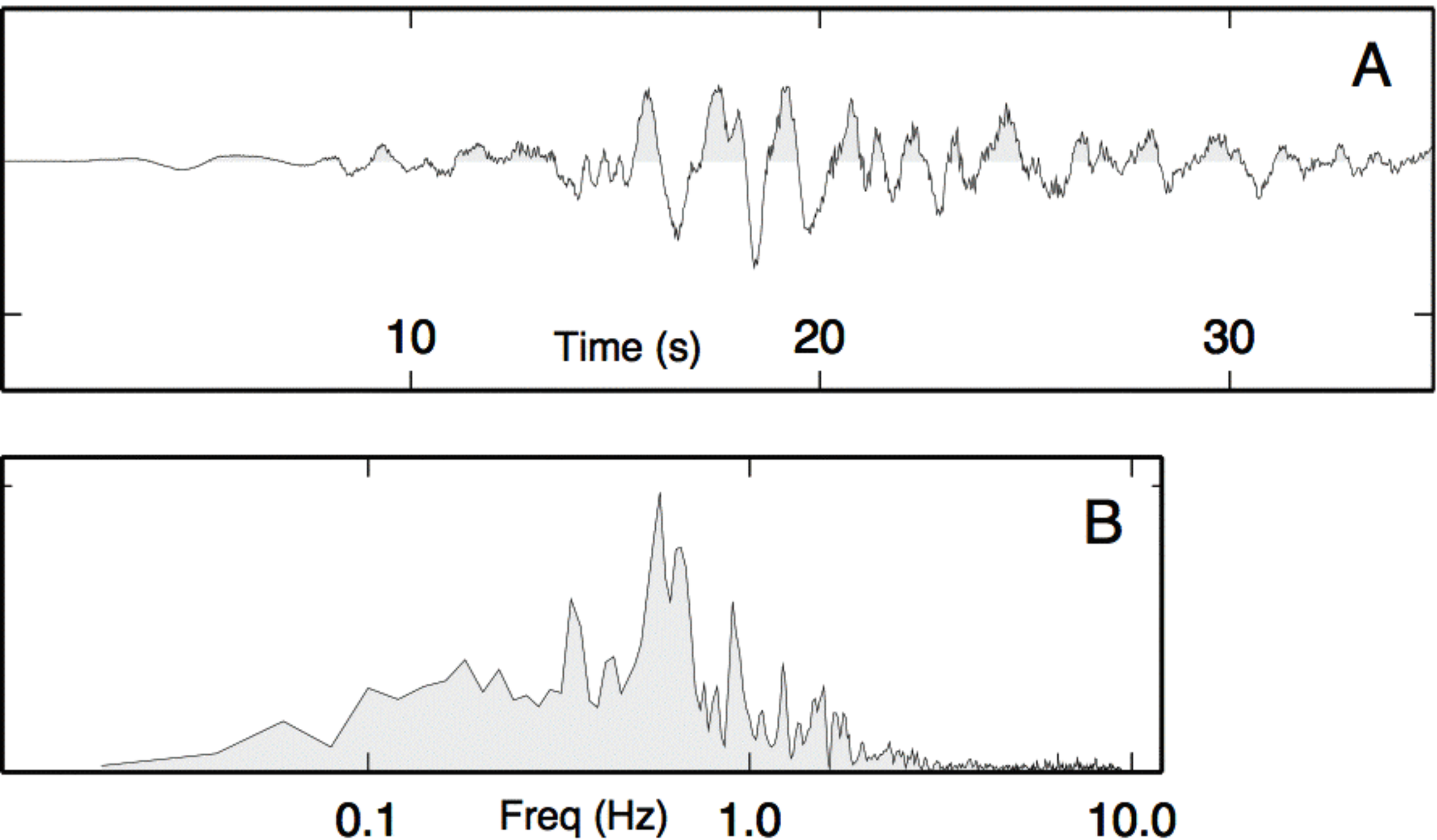
A
10
Time (s)
20
30
B
0.1
Freq (Hz)
1.0
10.0

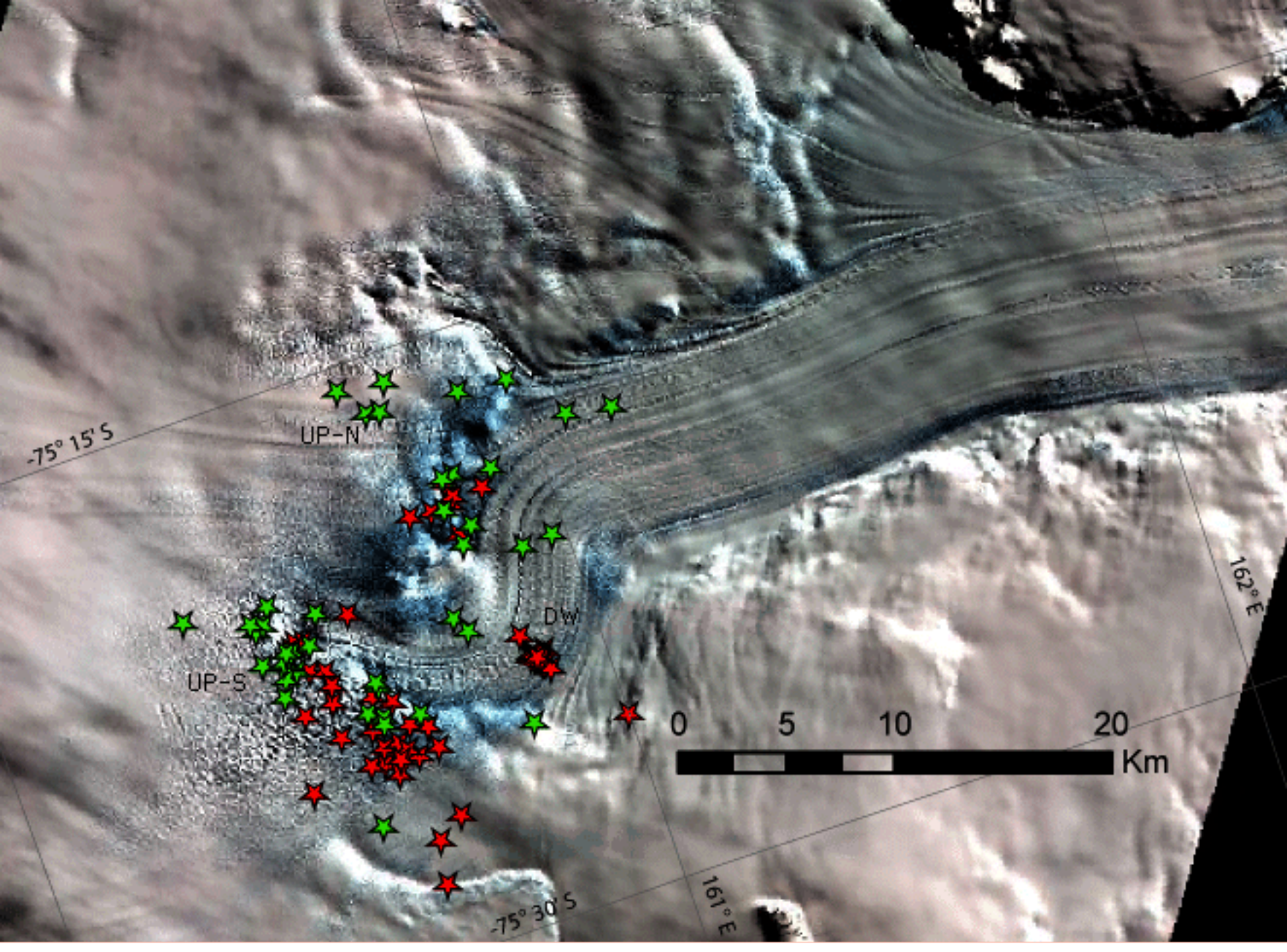
UP-N
DW
UP-S
-75° 15' S
-75° 30' S
161° E
162° E
0
5
10
20
Km

Magnitude Distribution

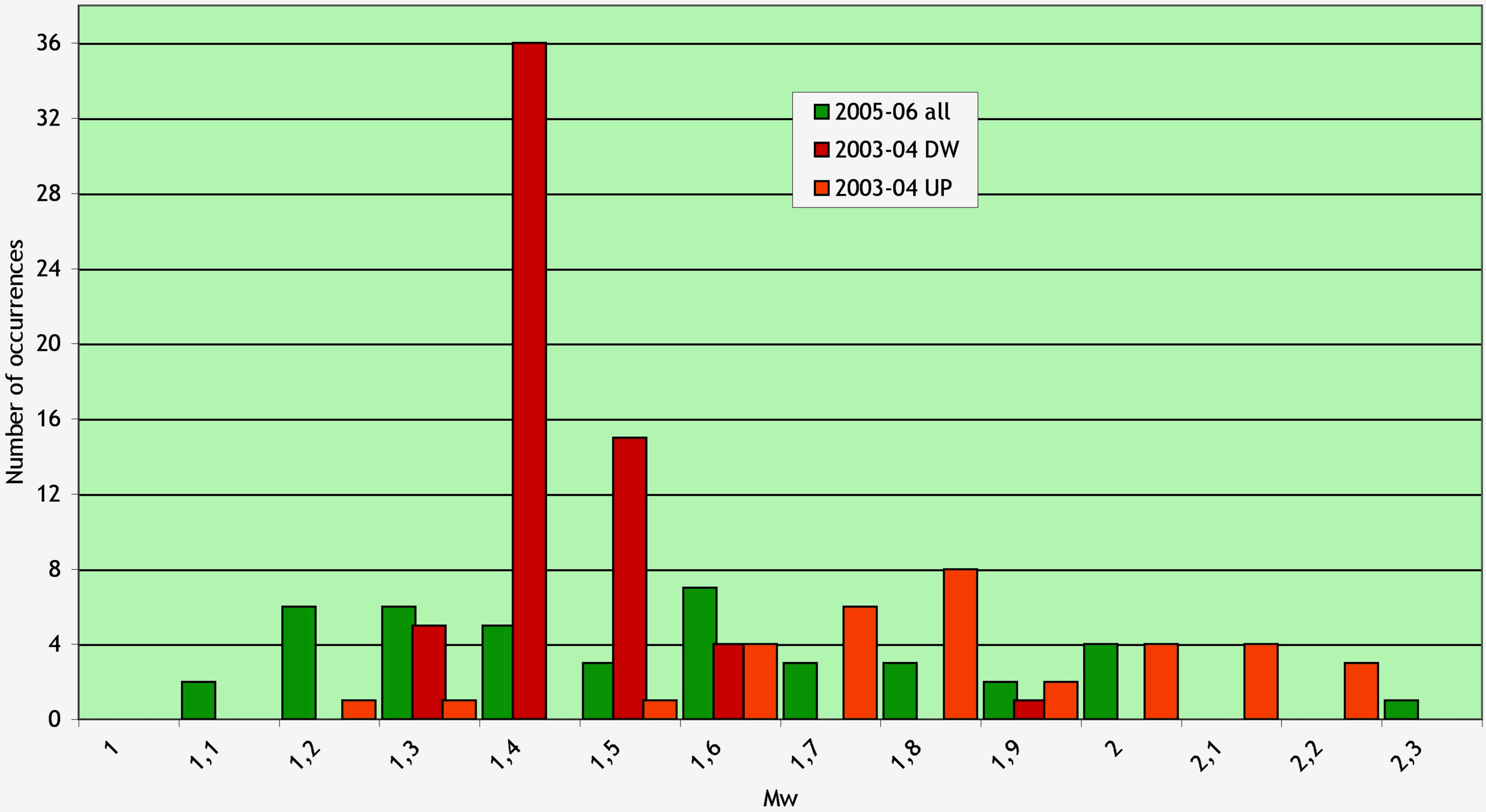

5
10
15
20
25
30
Time (s)

GPS Point ICF1 - Ellipsoidal Height (m)

202.00
201.80
201.60
201.40
201.20

GPS Point DRY1 - Ellipsoidal Height (m)

37.20
37.00
36.80
36.60
36.40
36.20
36.00

Predicted ocean tide (m)

0.6
0.4
0.2
0.0
-0.2
-0.4

1/11/06
1/15/06
1/19/06
1/23/06
1/27/06
1/31/06

Date

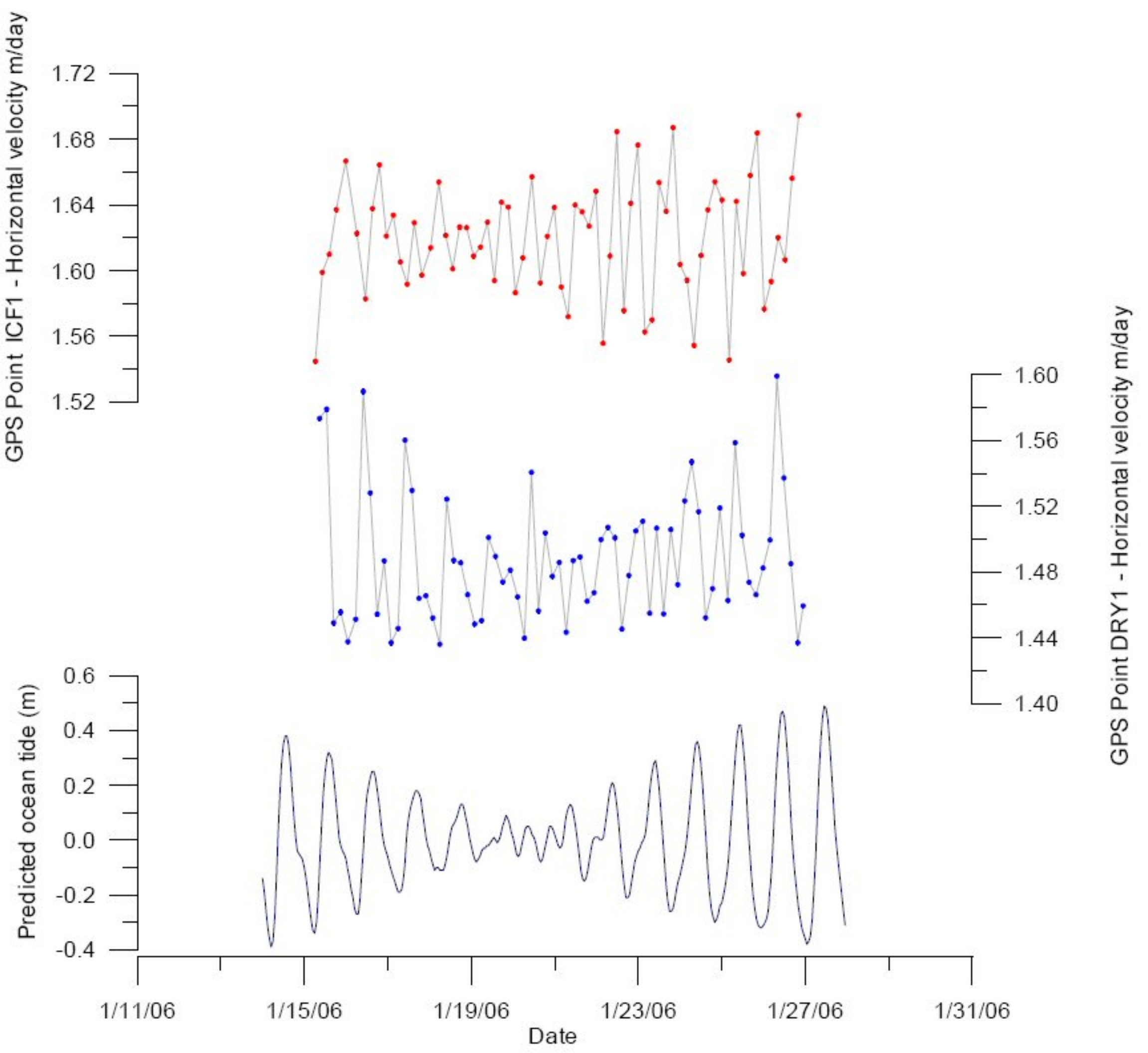
GPS Point ICF1 - Horizontal velocity m/day
1.72
1.68
1.64
1.60
1.56
1.52
GPS Point DRY1 - Horizontal velocity m/day
1.60
1.56
1.52
1.48
1.44
1.40
Predicted ocean tide (m)
0.6
0.4
0.2
0.0
-0.2
-0.4
1/11/06
1/15/06
1/19/06
1/23/06
1/27/06
1/31/06
Date